On the advantages of principal modes for multimode SDM transmission systems

Fabio A. Barbosa*, Filipe M. Ferreira
Optical Networks, Dept. Electronic & Electrical Eng., University College London, UK
**fabio.barbosa@ucl.ac.uk*

Abstract: MISO array size is shown to scale sublinearly with an increasing number of tributaries under modal dynamics and mode-dependent loss with up to 330 principal modes over a fibre optimised for low modal dispersion. © 2022 The Authors

1. Introduction

Spatial division multiplexing (SDM) has been proposed to cope with the ever-increasing transmission capacity demand while enabling the trend of reducing the cost per transmitted bit. There are several strategies for SDM implementation, and mode-division multiplexing (MDM) over multi-mode fibres (MMFs) offers the greater potential for spatial information density and, thus, potential integration in both system and component levels.

In MMFs, the co-propagating spatial channels interact to each other, being affected by new linear impairments, namely group delay (GD) spread [1], given the interplay between differential mode delay (DMD) and linear mode coupling, and mode dependent loss (MDL) [2]. GD-spread related effects can be undone by multiple-input multiple-output (MIMO) equalisation with complexity scaling with the total time spread, while MDL requires sophisticated equalisation schemes [3]. MMFs are generally designed with graded-index core in order to reduce DMD, but the greater the number of modes supported, the greater the minimum achievable DMD [4].

Conventional MDM transmission requires all guided modes to be detected for successful MIMO equalisation, which binds the number of transceiver front-ends to that of modes supported by the MMF. This averts the installation of large mode count (>>1) fibres, as it could not be feasible or economically viable to deploy transceivers with as many front-ends as fibre modes at system begin-of-life. Weakening this dependence would potentially enable multimode SDM to emulate the successful evolution of wavelength-division multiplexing, i.e. to use further channels as traffic demand grows. In the context of SDM, the number of tributaries N_T transmitted over a MMF with M spatial and polarisation modes could be scaled progressively. Essential attributes for decoupling the number of receivers from the number of supported fibre modes are reduced channel memory and suppressed modal crosstalk right at the front-end of coherent receivers. In [5], and for a $M = 12$ MMF, principal modes (PMs) were shown to have such characteristics while being suitable for high-baud rate transmission.

In this paper, we numerically investigate the use of PMs for a much larger number of spatial and polarisation modes, $M = 342$, under mode dependent loss and modal dynamics, and a varying rate of perturbations, while accounting for delay in the feedback of channel state information (CSI). The remaining modal coupling and the GD-spread for the residual channel are characterised when applying PMs.

2. Estimation of principal modes

In MMFs, and in the absence of MDL, PMs form a unique orthogonal multiplexing basis unaffected by modal dispersion (to 1st order) [6]. PMs correspond to the eigenvectors of a GD operator. Given the MMF channel, described by a frequency-dependent $M \times M$ matrix $\mathbf{H}(\omega)$, where M is the number of spatial and polarisation modes, the GD operator can be defined as [7]:

$$\mathbf{G}(\boldsymbol{\omega}) = \mathrm{j}\, \partial_{\boldsymbol{\omega}} \mathbf{H}(\omega) \mathbf{H}^{-1}(\omega) \tag{1}$$

The eigenvectors and eigenvalues of $\mathbf{G}(\boldsymbol{\omega})$ are, respectively, the input PMs $\mathbf{U}$ and their GDs $\tau_1, \ldots, \tau_M$. By forward

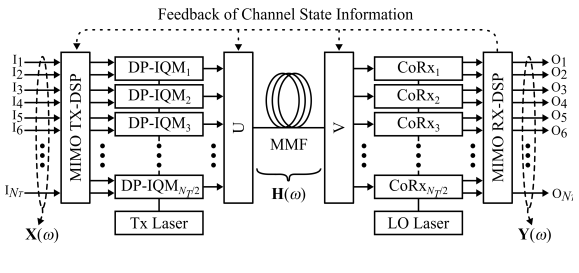

Fig. 1. Schematic diagram of the optical transmission system.

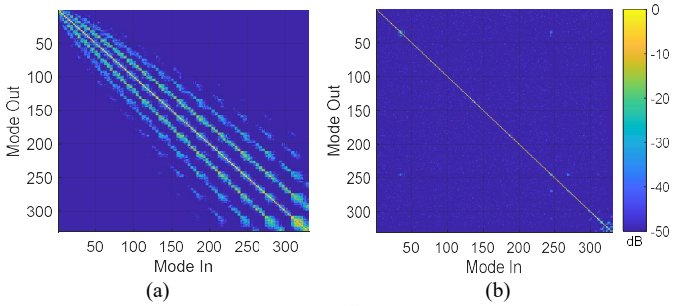

Fig. 2. Typical (a) $\mathbf{H}(\omega=0)$ and (b) $(\mathbf{V}^{\mathrm{H}})_{t=t_0}\mathbf{H}_{drifted}(\omega=0)(\mathbf{U})_{t=t_0}$, τ_{env} = 1 h.

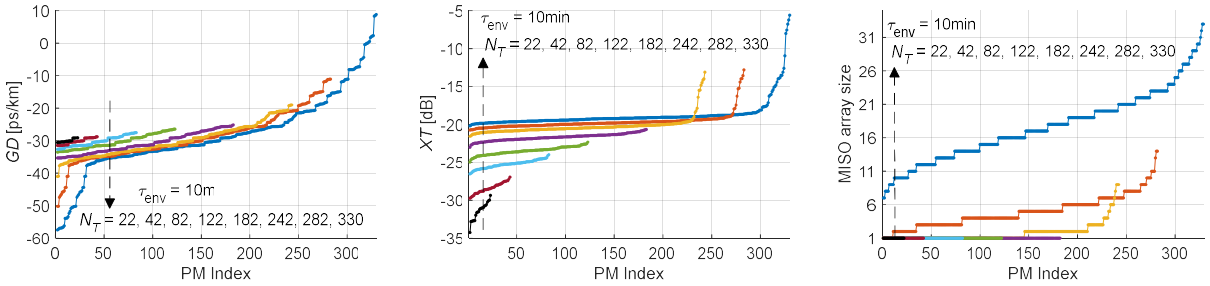

(a) (b) (c)

Fig. 3 For an increasing N_T, (a) *GD* and (b) *XT* per PM pair in a N_T-group. (c) MIMO array size required per PM pair to detect all data tributaries in a N_T-group. Results are sorted in ascending order for visualization purposes.

propagating **U**, we can calculate the output PMs **V**. PMs are frequency independent only to 1st-order, nevertheless coherence bandwidths of several THz have been shown for a wide range of M values [8]. Note that, each input PM in **U** has a correspondent output PM in **V**, i.e. an exclusive PM pair. Hereafter, PMs and PM pairs are used interchangeably.

The coherent SDM transmission system considered in this work is shown in Fig. 1. We assume CSI being feedback from receiver to transmitter with round trip delay τ_{rtt}. Input PMs **U** and output PMs **V** are exploited for mode multiplexing at the transmitter and for mode demultiplexing at the receiver, respectively. Both **U** and **V** are assumed to be applied in the optical domain using an ideal programmable mode multiplexer [9, 10]. By applying PM pairs (**U** and **V**) in the optical domain (as opposed to in the electrical domain), the channel memory and the extension of mode coupling are diminished at the receiver front-end [5] – potentially reducing to N_T (or $N_T/2$ for dual pol. receivers) the number of optical front-ends necessary to transmit&detect N_T spatial tributaries, importantly, where $N_T < M$. In the following, we transmit N_T tributaries over a $M = 342$ MMF using N_T optical front-ends at each.

2. Channel model

We calculate $\mathbf{H}(\omega)$ using the semi-analytical multi-section channel model in [11]. Here, we consider a 10-km MMF with $M = 342$ spatial and polarisation modes. Modelling includes all main linear impairments, Rayleigh scattering loss, macro-bend loss (MBL), DMD and linear mode coupling – along 1000 fibre sections of 10 m. All impairments are calculate for a graded-core trench-assisted fibre optimised following [4] for a refractive index contrast of 0.01 and a 45 μm radius. The MBL corresponding to one 60 mm radius loop is applied every section, leading to some of the modes in the last mode group to be "lost" (12 in total). The Rayleigh scattering loss ranges from 0.198dB/km for LP_{01} to 0.166 dB/km for the LP mode of the highest order. Fig. 2(a) shows a typical $\mathbf{H}(\omega = 0)$ (193.41 THz).

To investigate using PMs over a dynamic channel, $\mathbf{H}(\omega)$ is updated after the round-trip time that CSI has to travel τ_{rtt} using the drift model in [12]. The channel $\mathbf{H}(\omega)$ is perturbed by random skew-Hermitian matrices whose entries are given by a complex Gaussian distribution with variance $[\sigma_{drift}(\tau_{env})]^2 = k_D/\tau_{env}$, where τ_{env} is the desired timescale of change (same τ_{env} for all fibre sections) and k_D is a scaling factor that depends on the number of modes derived in [12]. Accordingly, the variance is increased linearly with time. The smaller τ_{env}, the greater the drift becomes, and the channel decorrelates faster with time. In summary, after calculating $\mathbf{H}(\omega, t = t_0)$ and the correspondent PM pairs **U** and **V**, a drift perturbation is applied to the channel, generating $\mathbf{H}_{drifted}(\omega) = \mathbf{H}(\omega, t = t_0 + \tau_{rtt})|_{\sigma_{drift}(\tau_{env})}$. **U** and **V** are then applied to transmit over $\mathbf{H}_{drifted}(\omega)$.

4. Results

In the following, τ_{env} ranges from seconds to hours, reflecting the long term stability of PMs reported in [8] (hours-to-months) as well as the typical acquisition time of $\mathbf{H}(\omega)$ using digital holography (i.e., ~0.1-to-100 s).

Fig. 2(b) shows the end-to-end residual channel when using all PM pairs (**U** and **V**) calculated for $\mathbf{H}(\omega = 0, t = t_0)$ to transmit over $\mathbf{H}(\omega, t = t_0 + \tau_{rtt})|_{\sigma_{drift}(\tau_{env})}$, with $\tau_{env} = 1$ h – smaller τ_{env} values are considered in the following. Reduced power off-diagonal terms in Fig. 2(b), dubbed here as *interfering terms*, are mostly caused by the mismatch between the PMs used and the drifted channel $\mathbf{H}_{drifted}(\omega)$. For $\tau_{env} = \infty$, it was verified that interfering terms were negligible, except for a small fraction of N_T-PM pairs (~1%) whose orthogonality was affected by MDL.

In a practical deployment scenario, the number of data tributaries required will increase progressively during the system lifetime. Thus, a strategy to select a group of N_T-PM pairs ($<M$) is required. Here, we simply select PM pairs by their GD deviation from the median value given all possible GDs, from lowest deviation onwards, to minimise any unwanted channel impulse response spread and so reduce equalisation complexity shall MIMO be required to untangle some of the data tributaries. Fig. 3 shows, for $\tau_{env} = 10$ min, the outcome of such selection strategy as the number of data tributaries is varied for $N_T = \{22, 42, 82, 122, 242, 282, 330\}$. For the sake of simplicity, data points

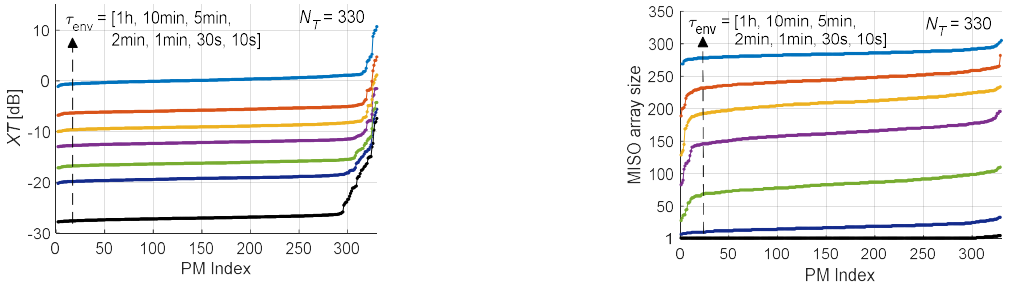

Fig. 4. For $N_T = 330$ and τ_{env} from 1h to 10s, (a) *XT* and (b) MIMO array size as a function of the PM index. Results are sorted in ascending order.

in Fig. 3 are presented in ascending order for each N_T. Fig 3(a) shows the *GD* for each PM pair that composes each group of size N_T. Fig. 3(b) presents the crosstalk (*XT*) per PM when all PMs of each group are used for transmission. As N_T increases, the overall level of crosstalk within the group also increases. For a given channel of interest, *XT* is the sum of the power of all *interfering terms* (visible in Fig. 2(b)) divided by the power of the respective channel.

To translate *XT* into the required multiple-input-single-output (MISO) array size per tributary, we count the respective *interfering terms*. For a given target signal-to-noise ratio (SNR), the weaker *interfering terms* are neglected. This is done by neglecting the smallest group of *interfering terms* that amounts to a *XT* below a certain threshold. Here, $XT \leq$ -20 dB. Thus, and after applying the required MISO, an *SNR* of 20dB is achievable should the channel additive noise allow. Fig. 3(c) shows the MISO array size for each PM pair in a group of N_T-PM pairs, with $\tau_{env} = 10$ min. For groups with 22, 42, 82, 122 and 182 PM pairs, single-input single-output (SISO) equalisation is sufficient for recovering the transmitted signals under the assumptions made in terms of XT and SNR. And, for groups with more than 182 PM pairs, MISO equalisation is necessary, although the maximum array size required for a given group, is at least an order of magnitude smaller than N_T. Note that, a linear scaling of the MISO array size with N_T would be for every PM pair in a group of N_T to require a MISO array size of N_T, i.e. $N_T \times N_T$ MIMO. Finally, a different grouping strategy that takes into consideration modal interference, rather than GD deviation from the median, can further reduce the equalisation array size requirements.

Fig. 4 (a) and (b) show the *XT* and MISO array size (required), respectively, as a function of the PMs index and for τ_{env} ranging from 1h to 10s. For τ_{env} from 1 min onwards, PMs no longer offer a sufficient XT suppression ($XT >$ -10 dB) which translates into a uniform MISO array size requirement comparable to N_T. Therefore, further investigation into the τ_{env} for MMFs (in lab and deployed conditions) is necessary. Nevertheless, in [8], PMs were found *quite stable* over many measurements in the course of 6 months. Moreover, the drift model followed here [12], was found to introduce *interfering terms* where mode overlap and effective index difference suggest otherwise (e.g., the off-diagonal grain pattern in Fig. 2(b)). Instead, a drift model accounting for environmental impact on the physical imperfections of the waveguide could be explore.

5. Conclusions

We have quantified how principal modes in MMFs allow increasing the number of data tributaries while sub-linearly scaling the MISO array size required. For a fibre with 342 spatial and polarization modes, the MISO array size required for a given group of N_T principal modes is found to be an order of magnitude smaller than N_T – for a characteristic channel drift time of 10 min. Further experimental characterisation and modelling of modal dynamics is required to fully understand the potential of principal modes in future high-throughput short-reach SDM systems.

This work was supported by the UKRI Future Leaders Fellowship MR/T041218/1. For the underlying data, see: doi.org/10.5522/04/21360492.

6. References

[1] C. Antonelli, A. Mecozzi, and M. Shtaif, "The delay spread in fibers for SDM transmission: dependence on fiber parameters and perturbations," *Opt. Express,* vol. 23, no. 3, pp. 2196-202, 2015, doi: 10.1364/OE.23.002196.
[2] K.-P. Ho and J. Kahn, "Mode-dependent loss and gain: statistics and effect on mode-division multiplexing," *Opt. Express* 19, 16612, 2011.
[3] E. Chou and J. Kahn, "Successive Interference Cancellation on Frequency-Selective Channels With Mode-Dependent Gain," *IEEE/OSA JLT* 40, 3729, 2022.
[4] F. Ferreira, et al., "Design of few-mode fibers with M-modes and low differential mode delay," *IEEE/OSA JLT* 32, 353, 2014.
[5] F. A. Barbosa and F. M. Ferreira, "Scaling Spatial Multiplexing with Principal Modes," in *IEEE IPC*, 2022, p. WF1.3.
[6] S. Fan and J. M. Kahn, "Principal modes in multimode waveguides," *Opt. Lett.* 30, 135, 2005.
[7] D. Askarov and J. M. Kahn, "Long-Period Fiber Gratings for Mode Coupling in Mode-Division-Multiplexing Systems," *IEEE/OSA* 33, 4032, 2015.
[8] J. Carpenter, et al., "Observation of Eisenbud–Wigner–Smith states as principal modes in multimode fibre," *Nat. Photon.* 9, 751, 2015.
[9] N. K. Fontaine *et al.*, "Programmable Vector Mode Multiplexer," in *2017 (ECOC)*, 17-21 Sept. 2017 2017, pp. 1-3, doi:.
[10] D. Pohle, et al., "Intelligent Self CalibrationTool for Adaptive Mode Multiplexers using MultiplaneLight Conversion," in *ICO*, 2022.
[11] F. M. Ferreira, et al., "Semi-Analytical Modelling of Linear Mode Coupling in Few-Mode Fibers," *IEEE/OSA* 35, 4011, 2017.
[12] K. Choutagunta, et al., "Efficient Quantification and Simulation of Modal Dynamics in Multimode Fiber Links," 37, 1813, 2019.